Intensification of highly exothermic fast reaction by multi-injection microstructured reactor

J. Haber[1*], B. Jiang [2,3], T. Maeder[2], N. Borhani[4], J. Thome[4], A. Renken[1], L. Kiwi-Minsker[1*]

[1]Group of Catalytic Reaction Engineering (GGRC)
[2]Laboratory of Microengineering for Manufacturing 2 (LPM 2)
[3]Ceramic Laboratory (LC)
[4]Laboratory of Heat and Mass Transfer
Ecole Polytechnique Fédérale de Lausanne (EPFL), CH-1015 Lausanne, Switzerland
*Email: lioubov.kiwi-minsker@epfl.ch

Version of record: Chemical Engineering and Processing: Process Intensification, 2014.
http://hdl.handle.net/10.1016/j.cep.2014.02.007

ABSTRACT

Microstructured reactors (MSR) with characteristic dimensions below 100 μm are warranted to maintain close to isothermal conditions when carrying out quasi-instantaneous highly exothermic reactions. Unfortunately, such small dimensions increase the risk of clogging, create high pressure drop and are costly to number-up. The multi-injection (MI) MSR, where one of the reactants is added stepwise along the reactor length, allows working with larger dimensions (diameter >500 μm) while maintaining good temperature control. Herein presented MI-MSR is made of low temperature co-fired ceramics (LTCC) with herringbone mixing structure inside the reactor channels and is shown to mix efficiently in a large range of Reynolds numbers Re = 20‑130. The cyclization of pseudoionone is studied as a model of a highly exothermic fast reaction. The temperature profiles are characterized by a quantitative infrared thermography. The developed LTCC MI-MSR allows ~8-fold reduction of hot spot temperature as compared to the adiabatic temperature rise. Moreover, ~500-fold intensification is achieved as compared to the conventional semi-batch process with reduced solvent mass by a factor of 2 while attaining a yield of target product above 98%.

Keywords: Process intensification; Microstructured reactor; Multi-injection; infrared thermography; Exothermic reaction; Cyclization of pseudoionone

Nomenclature

a	specific surface area, [1/m]		B	fit variable, [1/m^2]
C	fit variable, [W/(m^3 K)]		C'	fit variable, [W/(m^3 K)]
c	concentration, [mol/m^3]		c_p	heat capacity, [J/(kg K)]
d_h	hydraulic diameter, [m]		h	height of the void channel, [m]
H_r	reaction enthalpy, [J/mol]		k	rate constant, [(m^3/mol)$^{n-1}$/s]
L	channel length, [m]		M	fit variable = C/B, [W/(m K)]
n	reaction order, [-]		N	amount of units used for numbering-up, [-]
q	groove wave factor, [-]		Q	volumetric flow rate, [m^3/s]
R	volumetric heat transfer resistance, [(m^3 K)/W]		t_c	characteristic cooling time $\rho \cdot$ cp/Uacool, [s]
tm	characteristic mixing time, [s]		t_r	characteristic reaction time 1/(k$\cdot$ c$_0$n^{-1}), [s]
T	temperature, [K]		u	flow velocity, [m/s]
$Ua_{global}l$	global volumetric heat transfer coefficient, [W/(m^3 K)]		Ua_{loss}	global heat losses to surrounding coefficient, [W/(m^3 K)]
V	volume, [m^3]		W	channel width, [m]
x	abscissa, [m]		X	conversion, [-]
Y	yield, [-]		z	axial coordinate, [m]
z'	axial coordinate, [m]			
Greek				
α	factor describing the ratio of herringbone height to void channel height, [-]		α	designates the α-ionone molecule
$\alpha(H^+)$	designates the α-ionone molecule in its protonated state		β	designates the β-ionone molecule
$\beta(H^+)$	designates the β-ionone molecule in its protonated state		λ	thermal conductivity, [W/(m K)]
Δ	symbol for difference		θ	uncalibrated temperature shown by the infrared camera, [°C]
ρ	mean density, [kg/m^3]		τ	residence time, [s]
Dimensionless numbers				
$DaII_{mix}$	Mixing Damköhler number tmix/tr		Re	Reynolds number u$\cdot$ dh/ ν , [-]
Subscript				
0	initial condition		ad	adiabatic
c	in the cooling layer		iso	isopropanol
loss	related to heat losses		LTCC	low temperature co-fired ceramics
MSR	microstructured reactor		PI	pseudoionone
S	surrounding		Wall	wall

1 Introduction

The high heat transfer rates achieved in microstructured reactors (MSR) [1] render this type of equipment ideal to control temperature of rapid exothermic reactions and to accelerate the kinetics of chemical reactions by increasing temperature and/or pressure [2-4]. Nevertheless, quasi-instantaneous reactions with characteristic reaction times $t_r = 1/(k \cdot c_0^{n-1})$ below 1 s, such as organo-metallic, acid-base or the presented cyclization reaction require special consideration. To obtain close to isothermal conditions for this type of reactions, the reactors with hydraulic diameters (d h) below 100 µm are needed [5]. Such small characteristic dimensions inevitably lead to high pressure drop and channel clogging, which makes it difficult to implement such equipment on industrial scale. Moreover, when numbering-up [1, 6, 7], the amount of channels N needed to attain the target throughput increases with $1/d_h^2$:

$$N = \frac{Q_{\text{target}}}{Q_{\text{1 channel}}} = \frac{V_{\text{target}}}{V_{\text{1 channel}}} \propto \frac{1}{d_h^2} \tag{1}$$

The continuous multi-injection (MI) reactor [8-11] presents an option to circumvent the drawbacks of small channels. In analogy to the semi-batch reactor, one of the reactants is added stepwise along the reactor length [1]. By varying parameters such as the amount of injection points and the flow rate of dosed reactant, the heat production, and in turn the temperature profile can be controlled. While this type of reactor prevents the use of excessively small channel dimensions, as trade-off one has to accept a broadened residence time distribution due to the injected flow and a high pressure drop related to the flow distribution [1].

To ensure the efficient temperature control within a MI-MSR, at least 90% of the dosed reactants have to be transformed before the subsequent injection point. For fast reactions, the overall rate of transformation depends not only on the intrinsic kinetics, but also on the mixing efficiency. Depending on the ratio of characteristic mixing time and characteristic reaction time $t_{\text{mix}}/t_{\text{r}}$, i.e. the mixing Damköhler number $DaII_{\text{mix}}$, the overall reaction kinetics differ:

- $DaII_{mix} = t_{mix}/t_r \leq 0.01$·: No influence of mixing on the overall transformation rate
- $DaII_{mix} = t_{mix}/t_r \leq 0.1$: Negligible influence of mixing on the overall transformation rate
- $0.1 \leq DaII_{mix} = t_{mix}/t_r \leq 10$: Overall transformation rate is influenced by mixing of the reactants
- $DaII_{mix} = t_{mix}/t_r \geq 10$: Overall transformation rate is controlled by mixing of the reactants

When working with rapid exothermic reactions with characteristic reaction times smaller than 1 s, in many cases mixing time which is in the order of milliseconds to seconds [12] cannot be neglected. Therefore, mixing of the reactants plays an essential role in the formation of temperature profiles in a MI-MSR.

In the present work, a multi-injection MSR is developed to carry out the exothermic and quasi-instantaneous model reaction, i.e. the cyclization of pseudoionone to α- and β-ionone. Thereby, the objective is two-fold:

1) Characterization of the temperature profile in a MI-MSR.
2) Intensification of the model reaction aiming at the optimization of the yield of ionones and of the product distribution.

2 Experimental

The experimental chapter is split into three sections: 1) A brief description of the model reaction is followed by 2) the development of the multi-injection reactor using LTCC technology, before showing 3) the two methods of characterization used in the present study.

2.1 Model Reaction

The cyclization of pseudoionone to α- and β-ionone is a complex reaction and takes place only in the presence of sulfuric acid. The product distribution is strongly sensitive to temperature and acid concentration (see Fig. 1). Due to the very fast kinetics, mixing plays a crucial role since the acid concentrations influence product distribution and the global transformation rate. The target products, α- and β-ionone, are used in perfumery and in the synthesis of vitamin Kashid et al. proposed a reaction scheme and investigated the kinetics including the different reaction steps under homogeneous conditions using 1-nitropropane as solvent [13] and [14].

A simplified scheme of the cyclization of pseudoionone is given in Fig. 1 with the corresponding structural formulas in Fig. 2. Thereby, concentrated sulfuric acid is added in over-stoichiometric amount to the reaction mixture with a molar ratio of acid to pseudoionone of 4.8:1 in order to obtain full conversion [14]. Pseudoionone gets protonated quasi-instantaneously with a heat release of $\Delta Hr = -71$ kJ/mol, followed by the very fast cyclization (−57 kJ/mol) to form a cyclized intermediate. Kashid et al. characterized the two first reaction steps, whose quasi-instantaneous intrinsic kinetics are difficult to monitor [13]. Hence, temperature control during the two first reaction steps is challenging. The intermediate molecule obtained from the latter steps is in equilibrium with the protonated form of α-ionone, and is irreversibly transformed to protonated β-ionone. The isomerization from the protonated α-ionone molecule to the protonated β-ionone is only slightly endothermic (8 kJ/mol), and therefore, not critical from the thermal point of view. The reaction can be simply quenched by the addition of water, where α-ionone and β-ionone are obtained in separate phases.

Moreover, it is very important to avoid high temperatures, which trigger the consecutive polymerization of the product. On the one hand, it leads to a loss of yield, and on the other hand, this highly exothermic step can give rise to a dangerous run-away of the reactor. To suppress the consecutive polymerization, and, in turn, maximize the yield of α-ionone β-ionone, the temperature control of this reaction was done by application of the MI-MSR.

Two homogenously miscible inlet solution were prepared for the experiments using 1-nitropropane as solvent:

- Pseudoionone solution: 1.2-2.75 M in 1-nitropropane
- Sulfuric acid solution: 7.5-12 M sulfuric acid in 1-nitropropane

Upon the mixing these solutions give an adiabatic temperature rise of $\Delta Tad = 36\text{-}85°C$ depending on the concentration. Thereby, the ratio of acid to pseudoionone was varied between a value of 6 and 2.7. The physical properties of the pure reactants at 25°C are summarized in Table 1 together with the estimated properties of the solutions (denoted by *) [5].

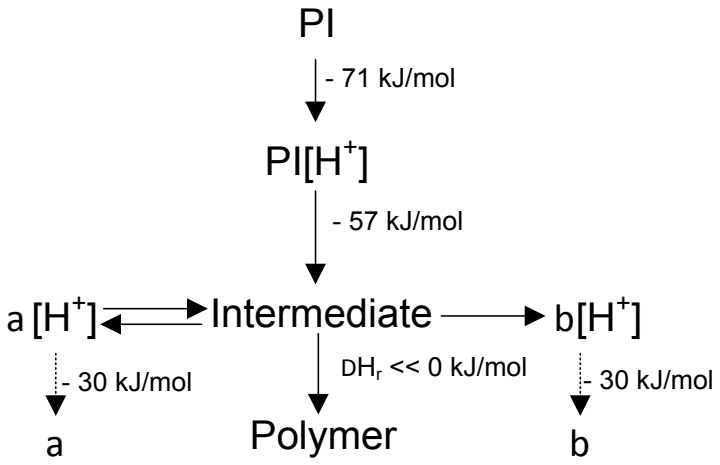

Figure 1: Reaction network with enthalpies proposed by Kashid *et al.* [14]. PI: pseudoionone, α: α-ionone β: β-ionone. The reaction enthalpy of – 30 kJ/mol is obtained by superposition of the deprotonation enthalpy (71 kJ/mol) and the enthalpy released by the dilution of sulfuric acid to 60 % w/w. The isomerization from α[H^+] to β[H^+] is slightly endothermic with ΔH_r = 8 kJ/mol.

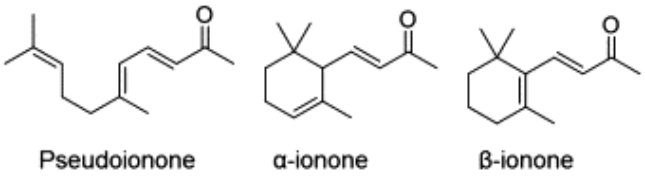

Figure 2: Structural formulas of pseudoionone, α -ionone and β -ionone.

Table 1: Physical properties of the compounds at 25 °C used for the homogeneous cyclization of pseudoionone [5, 15, 16]. The properties of α-ionone are assumed to be similar to β-ionone.

	Density [kg/m^3]	Heat capacity [J/(kg K)]	Kinematic viscosity [m^2/s]
1-Nitropropane	998	1972	$7.90 \cdot 10^{-7}$
Pseudoionone	895.1	1930	$6.38 \cdot 10^{-6}$
β-ionone	940	-	$1.15 \cdot 10^{-5}$
Sulfuric acid	1840	1340	$1.34 \cdot 10^{-5}$
Solution A*	970	1962	$2.17 \cdot 10^{-6}$
Solution B*	1372	1596	$8.28 \cdot 10^{-6}$
Product mixture*	1169	1757	$5.60 \cdot 10^{-6}$

*Calculated properties assuming an initial solution of 1.25 M of pseudoionone and 7.5 M of sulfuric acid.

2.2 Development of the Multi-Injection Reactor

For the design of the MSR, low temperature co-fired ceramics (LTCC) technology was selected. The materials and manufacturing process are introduced, and the three reactor designs are presented: two distinct mixing structures are built for comparison; subsequently, the most efficient structure (the herringbone structure) is embedded into the final MI-MSR.

2.2.1 Low Temperature Co-fired Ceramics

Low temperature co-fired ceramics (LTCC) was chosen to build up the ceramic MI-MSR. In the thick-film technology area [17], LTCC is used for the creation of electronic substrates for high frequency applications. To ensure compatibility with low-cost, high-conductivity silver-rich conductors, the sintering process of LTCC ("co-firing" of the electrode and the substrate) has to ensure complete densification below ~950°C (hence the term "low", as opposed to "high" for the analogous HTCC technology). Typically, the maximum dwell temperature in the firing cycle lies between 800°C and 900°C. The key advantages of LTCC for its use as microstructured reactor are the following:

- High corrosion resistance towards strong acids and bases achieved by some compositions [18]
- Due to the high precision obtained with laser ablation, fine structures with dimensions less than 200 μm can be created depending on laser type.
- The stacking procedure enables the creation of three dimensional superposed structures.
- The low achievable thickness of the layers essentially nullifies the heat transfer resistance in the wall as compared to the resistance within the reaction channels resulting in high heat transfer rates.

Fig. 3 shows a simplified fabrication scheme of the LTCC reactor [19]. It is fabricated out of several plain layers of LTCC tapes, which are commercially available in different thicknesses between 50 and 250 μm. The commercial glass-ceramic composition DuPont 951 was chosen for the construction because of its chemical inertness [18, 20, 21]. Because it is mainly composed of Al_2O_3 and glass, its chemical resistance is comparable to that of borosilicate glasses [18]. The designed channel patterns are applied by means of laser ablation (1064 μm Nd:YAG, LS9000 Laser Systems GmbH) (A). Subsequently, the tapes are stacked together using an alignment setup, leading to a 3-dimensional structure (B). The lamination of the stacked tapes was achieved through the novel progressive lamination process that not only enables inter-penetration of ceramic particles in the LTCC by diffusion of the organic binders, but, also guarantees the quality of embedded cavities (C) [20]. The firing of the stack generally occurs in two steps: (1) removal of the organics via evaporation and oxidation at about 400°C, followed by (2) liquid-phase sintering [22] of the ceramic layers up to ~900°C [19] (D), often accompanied, towards the end, by internal reactions and crystallization processes [23] and [24]. Thereby, a homogeneous shrinkage of the reactors of 30% (±2%) has to be taken into account in the direction normal to the surface. In the final steps, the reactor is cut to size and the fluidic connections are made (E, F).

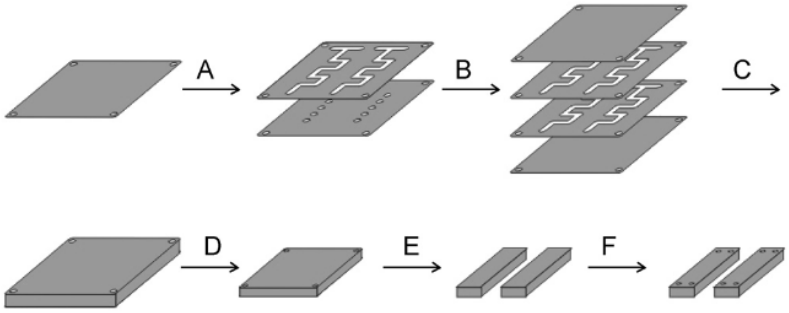

Figure 3: Scheme of the fabrication of LTCC microstructured reactors. (A) Structuring by laser ablation; (B) Stacking of the layers; (C) Isostatic lamination; (D) Firing; (E) Dicing; (F) Fluidic opening by laser ablation. Image adopted from Große *et al*. [21].

2.2.2 Micromixing structures of LTCC

Several mixing structures can be found in the literature [25] and [26] among which two distinct designs were chosen: the tangential mixer [26] and [27] and the herringbone mixer [28], [29], [30], [31], [32] and [33]. While the tangential mixer turned out to require high Reynolds numbers ($Re = u \cdot d_h/\nu > 100$) to achieve good mixing quality, the herringbone mixer is one example of a structure providing efficient mixing at low Reynolds number. Both structures were manufactured on 25 mm × 62 mm plates using LTCC and tested regarding their suitability for the integration in the MI-MSR (see Section 2.2.3).

Within the tangential mixer, the fluid flows through a series of narrow channels followed by a recirculation zone (Fig. 4A). The recirculation increases the mixing quality with increasing Reynolds number [27]. In the ideal case, this type of mixer can be assimilated to a cascade of continuous stirred tank reactors. As a consequence, when working with a number of structures less than 10 in series, one has to take into account a broader residence time distribution. For the present design, it was chosen to work with eight consecutive recirculation zones with a diameter of 2 mm (viewed from the top) and a channel height of 500 µm. The width of the transfer channels connecting one zone with the following was set to 500 µm. The Reynolds number in the present study was defined in the narrow section, where dh = 500 µm. The total reactor volume from the contact point of the reactants to the reactor outlet is 18 µl.

In the herringbone mixer, the addition of grooves on the bottom of the channel induces a flow velocity component that is normal to the flow direction [29-33]. By alternating the direction of the grooves, the two inlet flows are successively "folded" on top of each other even at low Reynolds number ($Re < 10$). For the present herringbone mixer, 7.5 cycles of 10 grooves per half cycle were built up. The groove thickness is 100 µm with a space of 100 µm between the grooves ($2\pi/q = 200$ µm). The channel cross section is 530 µm × 500 µm ($(h + h \cdot \alpha) \times W = H \times W$) with $\alpha = 0.30$ being the ratio of the height of the herringbone to the height of the open channel (excluding the herringbone). The mixer with a total channel length of L = 68 mm and a volume of approximately 19 µl is depicted in Fig. 4B.

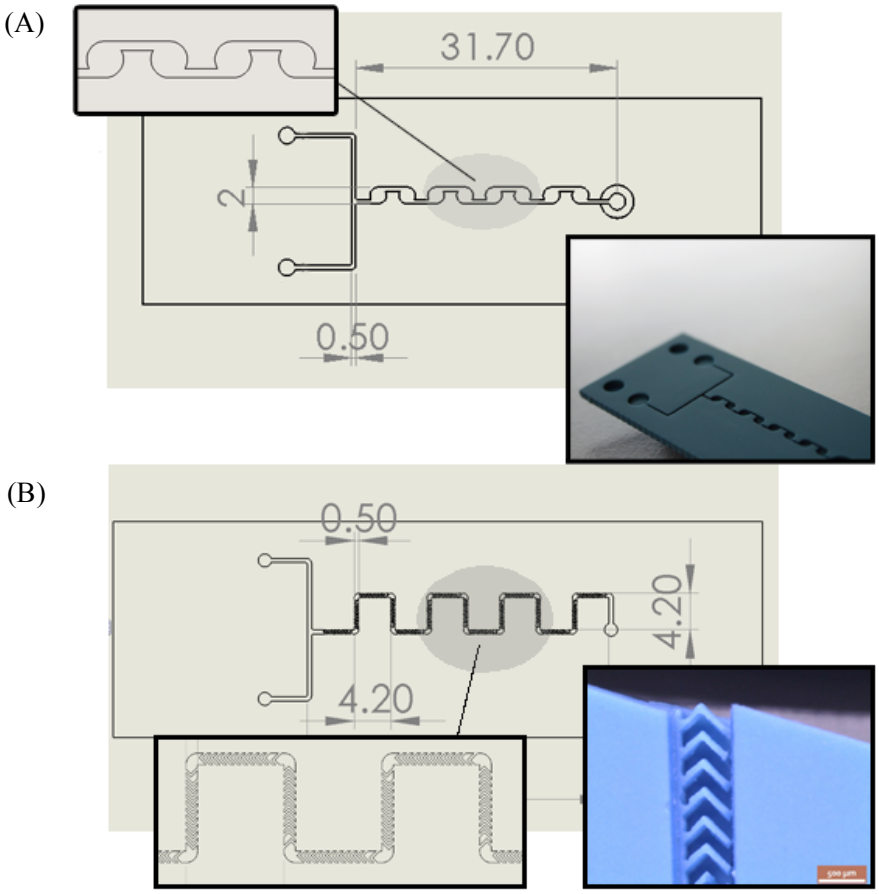

Figure 4: Scheme of the tangential mixer (A) and the herringbone mixer (B). The dimensions are given in millimeter.

2.2.3 Multi-injection Microstructured Reactor from LTCC

The reactor was constructed out of a total of 11 layers of ceramic green tape (Dupont 951). Some of these layers are identical to each other which is used to built-up the required thickness: e.g. to obtain an overall height of the herringbones of ~150 µm (before shrinkage), 3 layers of 50 µm are needed. After firing, shrinkage of the layer thicknesses of ~30% has to be considered. Hence, 8 different structures were created by laser ablation (see Fig. 5), and are shortly described in the following starting from the top layer. The thicknesses are given in the unfired state:

1) The connection plane (156 µm) contains an overall of 11 holes with a diameter of 1 mm allowing all the connections to be done from the top of the reactor.
2) The channel layer (508 µm) creates the void space above the herringbone structures. Together with the herringbone layer, the resulting cross section is 560 µm × 500 µm ($(h + h{\cdot}\alpha) \times W$) in the mixing module and 560 µm × 2000 µm in the residence time module. Thereby, the residence time module provides residence time for the evacuation of heat and for the transformations of the non-instantaneous reaction steps. The total length of one mixing module is 66 mm followed by 33 mm of residence time module before reaching the subsequent injection point.
3) The herringbone layer (150 µm) contains a total of 7 cycles of herringbones with the same geometry as described in Section 2.2.2. Together with the channel layer, they form the reaction channels.

4) The cooling wall 1 (156 µm) separates the reaction channel from the cooling channel. Its low thickness provides almost no resistance to heat transfer between both channels.
5) The cooling layer (508 µm) contains three identical cooling channels having each 9 mm of width and about 5 cm of length. Each of these channels is exactly superposed to one single module of mixing and residence time channel of the herringbone layer. For manufacturing reasons, and to avoid maldistribution of coolant between the channels, this layer is fed by separate inlets.
6) The cooling wall 2 (254 µm) separates the cooling channel from the reactant inlet channel.
7) The inlet layer (508 µm) has the function to preheat the inlet flow before it reaches the first injection point located on the top of the reactor. The channel dimensions are identical to the dimensions of the residence time module.

For the mechanical stability of the green tape during the manufacturing process, the channels are crossed by "bridges". As their positions are shifted from one layer to another, the passage of the liquid is not hindered [34].

In Fig. 6 the fired MI-MSR is shown together with the device built to make the connections to the reactor.

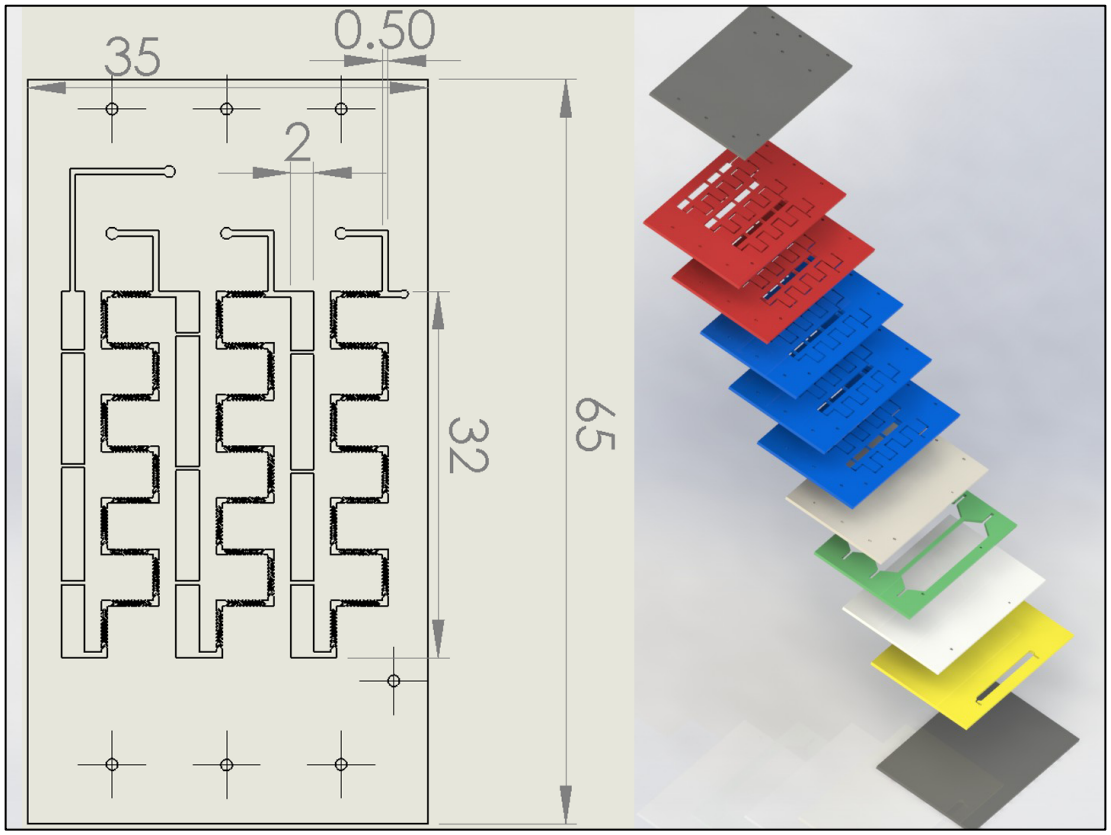

Figure 5: Scheme of the herrinbone layer of the multi-injection MSR containing the dimensions in millimeter (left), and the complete reactor built-up from 11 layers of green tape (right). From top to bottom: connection plane (grey), reaction channel (red), herringbone layer (blue), cooling wall 1(white), cooling layer (green), cooling wall 2 (white), inlet layer (yellow)

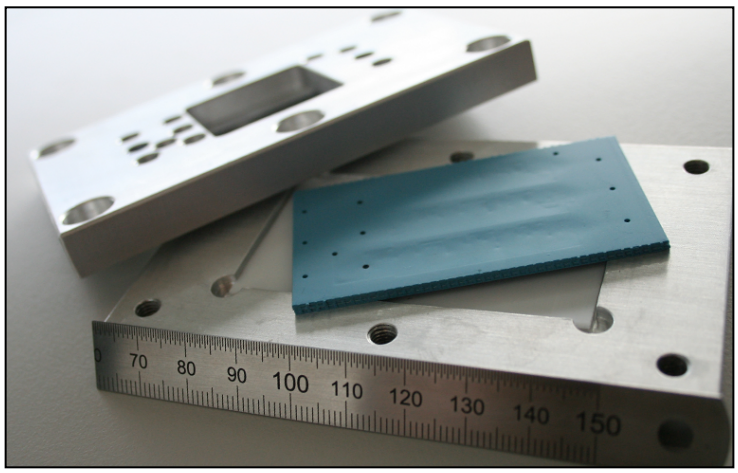

Figure 6: Device connecting the LTCC MI-MSR to standard 1/8 in. tubing using flangeless ferrules.

2.3 Methods of Analysis

The multi-injection MSR is plugged into a setup that is briefly addressed in the following. Two methods of characterization are available: the monitoring of axial temperature profiles within the microchannels and determination of product distribution by gas chromatographic analysis.

2.3.1 Experimental Setup

The temperature at each inlet and at the outlet is recorded with K-type thermocouples having a diameter of 500 µm. The values measured are used for the calibration of the infrared camera as described in Section 2.3.2. Moreover, pressure is monitored at the first inlet with pressure gauges with a working range of 0–28 bar and a precision of ±0.15 bar. With the abovementioned syringes, the maximal pressure that can be created lies in the order of 1 bar.

The setup used to carry out the experiments with the micromixers and the MI-MSR has been described in details elsewhere [5]. Each reactor inlet is fed with a separate syringe pump (KDS 100) equipped with Hamilton gastight syringes (50 ml), preventing maldistribution of the flows. The connections between the syringe pumps and the MI-MSR is made using 1/8 in. perfluoroalkoxy (PFA) tubes. The cooling circuit relies on a standard rotary vane pump, which was used to pump two different coolants through the heat exchange layer of the MI-MSR: water and isopropanol, respectively. Apart from their heat capacities ($c_{p,H2O}$ = 4180 J/mol and $c_{p,iso}$ = 2880 J/mol at 45 °C [15]), the main difference between both coolants is their thermal conductivity of 0.138 W/(m K) and 0.638 W/(m K) [15] at 45 °C.

2.3.2 Infrared Thermal Mapping

An infrared thermal imaging method was applied to monitor the axial temperature profiles of the MI-MSR. As the thickness of the top wall of the mixers and the reactor is <500 µm, the temperature on the reactor surface is approximately equal to the liquid temperature inside the reaction channel [16]. By combining such a reactor design with an external calibration of the infrared camera, which is carried out prior to the experiments, one can assess quantitative data of the temperature profile inside the microchannels with a resolution of 160 µm and a precision of ±1 °C.

In the present work, two distinct calibration methods have been applied. For the micromixers that were placed in a vacuum box to create quasi-adiabatic boundary conditions, a polynomial function was established for every pixel to relate the temperature inside the reaction channels Treal with the temperature observed by the camera, θ ("pixel-by-pixel calibration" [35]). As in the MI-MSR the heat losses were small compared to the heat exchanged with the cooling circuit, the vacuum box was omitted,

and a simpler calibration could be applied. Thereby, a homogeneous emissivity was assumed all over the reactor surface, which was determined by calibration at three distinct points [5].

2.3.3 Gas Chromatographic Analysis

After separating the organic phase from the aqueous phase, analysis of the product distribution was carried out via a Perkin-Elmer Auto System XL chromatograph equipped with a programmed split/splitless injector and a flame ionization detector employing a Stabilwax (Cross-bond Carbowax-PEG, Restek, USA) capillary column (i.d. = 0.32 mm, length = 30 m, film thickness = 0.25 μm). The calibration of the chromatograph was carried out with 90% (w/w) pseudoionone supplied by Aldrich, 96% (w/w) β-ionone supplied by Acros, and 90% (w/w) solution of α-ionone supplied by Aldrich. Thereby, the calibration curve was found to be quasi-identical for the three molecules. As internal standard, 99.5% (w/w) butanol (Alfa Aesar) was added to the sample before injection into the chromatograph.

The distribution of the products at the reactor outlet is characterized with a precision of ±5%. To obtain a representative product composition, the analysis of each sample is performed three times. As not all of the products can be detected, a mass balance analysis is performed after each experiment. Thereby, a deficit of the mass balance indicates either that the molecules are in an intermediate form (not monitored by the gas chromatograph) or have entered the unwanted consecutive polymerization. To distinguish both phenomena, the yield of the intermediate isomers 6,10-dimethylundeca-3,5-dione-10-hydroxy-2-one (denoted as intermediates') is used as indicator for the occurrence of the first type of mass balance deficit.

3 Results

This section is split into four parts. In the first part, the final choice of mixing structure is justified by comparing mixing efficiency of both mixers, and the effect of mixing quality on the product distribution in the MI-SR is studied. In the second part, the heat transfer in the MI-MSR is characterized, before showing temperature profiles with the reactive system in the MI-MSR and the resulting product distribution. Finally, the results obtained with reduced solvent (1-nitropropane) mass are presented.

3.1 Mixing Efficiency of the Structures

The selected structures have been shown to work efficiently with aqueous systems [25], [26], [28], [29], [30], [31], [32] and [33]. However, with the selected reaction system the considerable difference of density of the inlet flows ($\Delta\rho \approx 0.4$ kg/m^3) and the relatively high viscosity, as shown in Table 1, were found to render mixing an especially challenging task.

3.1.1 Comparison of Micromixers

To test the efficiency of the two mixing structures, the mixers were fed with solutions containing pseudoionone (1.2 M in 1-nitropropane) and sulfuric acid (7.5 M in 1-nitropropane) with an adiabatic temperature rise of $\Delta \mathrm{Tad} = 38\,^{\circ}$ C. Using the quantitative infrared thermal mapping method, the temperature profiles inside the channels were monitored to gain insight into the mixing phenomenon.

Supposing an ideally adiabatic mixer with a quasi-instantaneous reaction, the temperature rise inside the mixer is directly proportional to conversion of the reactants (see left term of Eq. (1)), which, in turn, is proportional to the degree of mixing. As the real mixers are not ideally adiabatic, the heat losses at the boundaries Ua_{loss} need to be defined. Especially at low flow rates, these losses play an important role when determining conversion [35]:

$$X = \frac{T - T_0}{\Delta T_{ad}} + \int_{z'=0}^{z'=z} \frac{Ua_{loss}}{\rho \cdot c_p} \cdot \frac{1}{u} \cdot \frac{\left(T - T_s\right)}{\Delta T_{ad}} \cdot dz' \qquad (2)$$

Here T designates the temperature inside the micromixer, T_0 the inlet temperature and T_s the temperature of the air surrounding the reactor. The flow velocity is denoted as u and $\rho \cdot c_p$ is the volumetric heat capacity of the mixture. The lumped volumetric heat loss coefficient Ualoss was estimated by flowing hot inert liquid (butanol) through the structure prior to the experiments, leading to values of 2.1×10^6 W/(m^3 K) and 1.4×10^6 W/(m^3 K) for the tangential and the herringbone mixer, respectively. In the curves presented in the following, the heat losses can be neglected when exceeding flow velocities of 0.15 m/s, as the second term in Eq. (1) becomes smaller than 10% of the first term.

The temperature profiles obtained for the tangential mixer are depicted in Fig. 7 for different linear velocities. For comparison, one should note that a total flow rate of 1 ml/min corresponds to a flow velocity of 0.067 m/s (in the narrow channel part), a residence time of about 1 s in the mixer and a Reynolds number of Re ≈ 10 (at the contact point, assuming an average viscosity of the mixture).

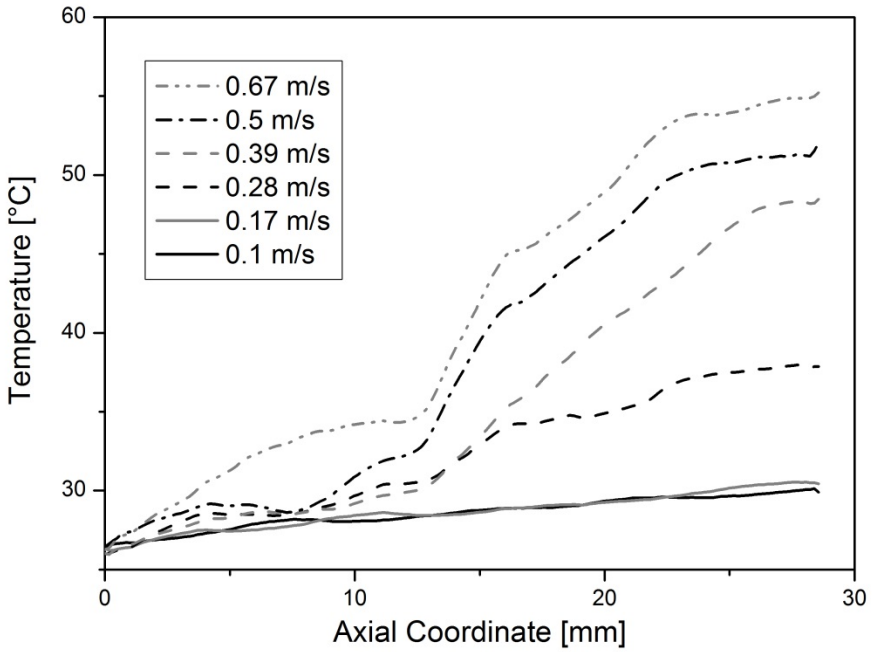

Figure 7: Mixing profiles obtained in the tangential mixing structure while mixing pseudoionone (1.2 M) with sulfuric acid (7.5 M).

For flow velocities lower than 0.17 m/s, almost no heat release is observed. In this regime, which is also entitled as stratified flow regime, mixing occurs almost solely by slow diffusion. Only when surpassing 0.28 m/s, a noticeable conversion (temperature rise) of the reactants is seen. This increased conversion indicates the appearance of first vortices, increasing the contact surface area between the two inlet flows. When exceeding velocities of 0.5 m/s (corresponding to Re ≈ 70), more than 50% of the adiabatic temperature is reached, while at 0.67 m/s already 80%, indicating almost complete mixing. Hence, a minimal Reynolds number of about 80 is required to efficiently mix with this structure.

The results obtained with the herringbone mixing structure are depicted in Fig. 8. As this reactor has approximately the same volume as the tangential mixer, the same approximation for Reynolds number and residence time holds.

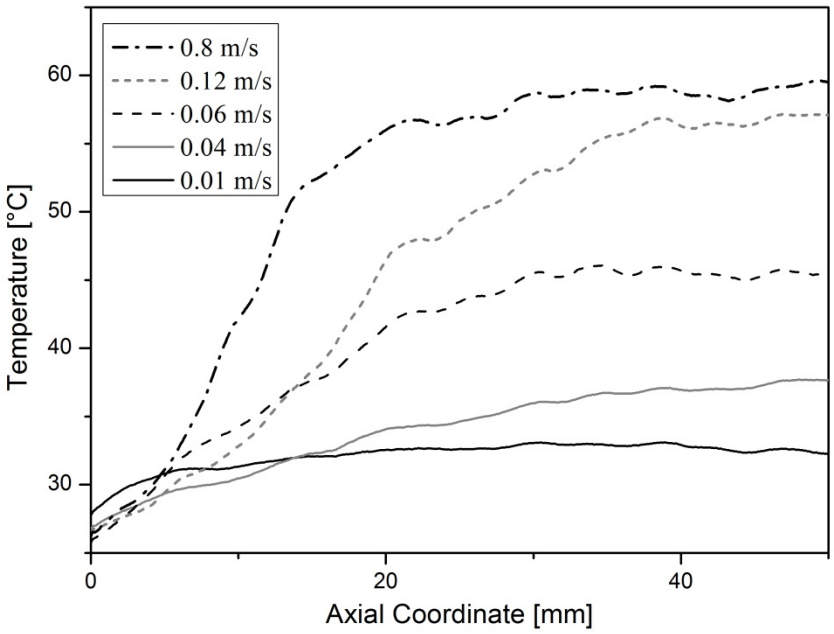

Figure 8: Mixing profiles obtained in the herringbone mixing structure while mixing pseudoionone (1.2 M) with sulfuric acid (7.5 M).

Compared to the tangential mixer, where an onset of the reaction is observed at a length of about 12 mm, this type of mixer leads to an immediate and almost linear increase in temperature. At flow rates as low as 2 ml/min (0.12 m/s), efficient mixing of the reactants is observed. This corresponds to a 4-fold reduction of the required Reynolds number compared to the previous structure. Moreover, when further reducing flow rate, a temperature rise up to 35 °C is observed. Thereby, because of the increasing importance of the heat losses, efficiency of the mixing process remains unclear. Nevertheless, using the latter structure, a much broader range of flow velocities is accessible, which was the reason for integrating the herringbone structure into the MI-MSR. Thereby, one has to keep in mind that a minimal Reynolds number of $Re = 20$ needs to be maintained to assure efficient mixing.

3.1.2 Mixing Efficiency and Product Distribution

In Fig. 9, the product composition at the outlet of the MI-MSR was determined at different flow velocities for a fixed coolant (isopropanol) temperature of 51 °C. The flow velocity is defined as the velocity in the mixing channel after the third injection point.

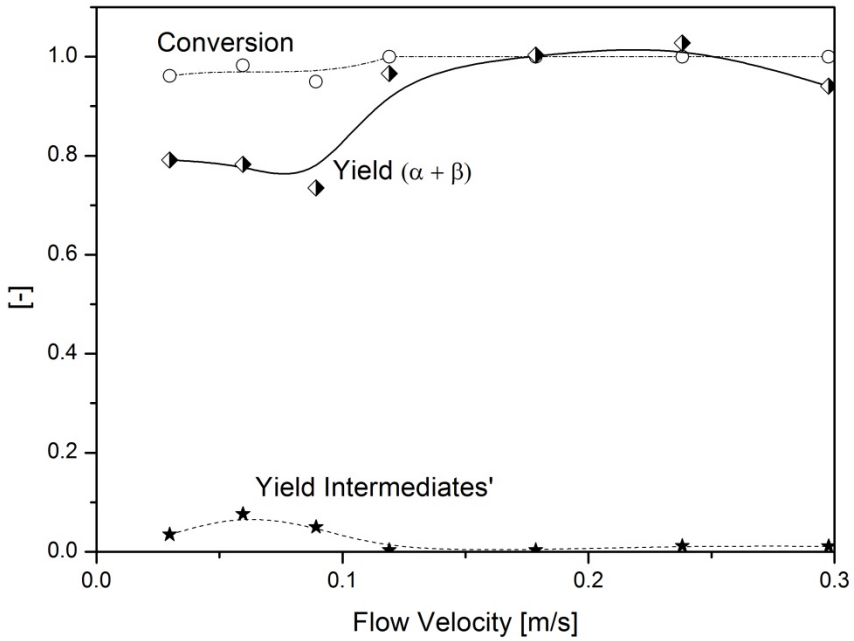

Figure 9: Yields and conversion at the outlet of the multi-injection MSR during cyclization of pseudoionone as function of flow rate. Coolant temperature: 51 °C, initial concentrations of the respective solutions: c_{PI} = 1.25 M; c_{H2SO4} = 7.5 M.

Over the velocity range studied conversion is above 0.95, with the lowest values being monitored at the lower range of flow velocities. A constant conversion of almost 1 is attained at flow velocities higher than 0.12 m/s. As in an ideal kinetically controlled system the conversion increases with the residence time, one can conclude that mixing strongly influences the transformation in this range of flow rates.

At a total flow rate of less than 2 ml/min (0.12 m/s) the inefficiency of mixing has an impact on the product composition, confirming the results reported in the previous paragraph. The yield of α-ionone and β-ionone is lower compared to the higher flow rates where a remarkable yield of $Y_{\alpha+\beta} > 98\%$ is achieved. The increased concentration of intermediates indicates that the loss of yield is due to the presence of intermediate molecules rather than due to the loss towards unwanted products of consecutive reactions. The increased segregation at lower flow rates leads to areas of low concentrations of acid. Kashid et al. [14] demonstrated that below a ratio of acid:pseudoionone of 2.4:1, the reaction cannot be completed.

3.2 Heat Transfer Performance

To evaluate the heat transfer performance between the heat exchange layer and the reaction layer, heat exchange experiments were carried out. Thereby, the channels on the reaction layer are fed with ethanol/butanol (via the first injection point) at room temperature. The latter are heated up by the heat exchange medium passed with a temperature of 40 °C/50 °C. Two different media were used: isopropanol and water. As the heat losses by radiation and convection are neglected for the estimation of the volumetric heat transfer coefficient, the value obtained from the described experiment is a superposition between the actual heat transfer coefficient and the heat losses to the surroundings. Hence, the real heat transfer coefficient between the reaction and the heat exchange layer is always higher. A typical profile with ethanol in the reaction channel and water in the cooling channel is presented in Fig. 10.

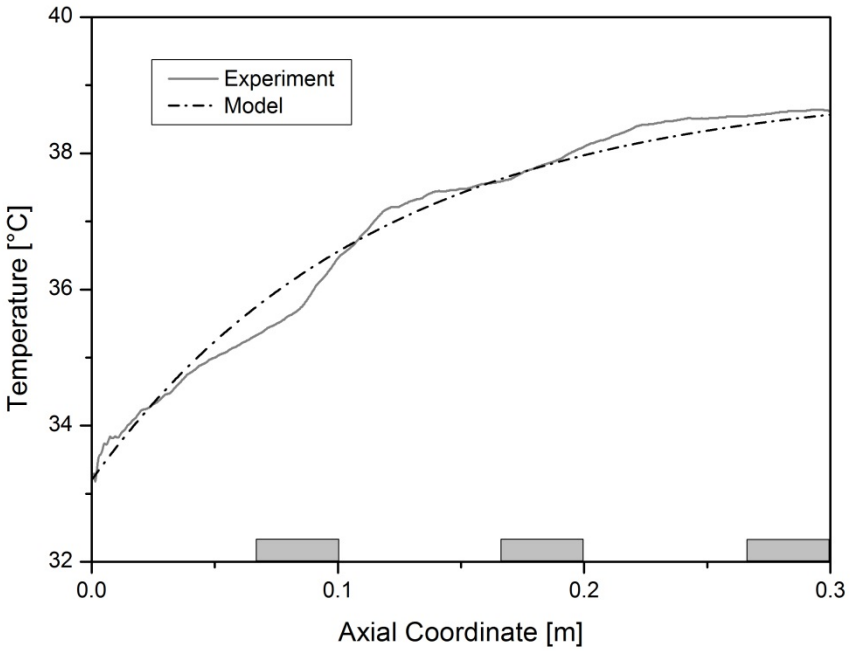

Figure 10: Temperature profile measured and modeled in the MI-MSR using a simple heat transfer model with constant heat exchange medium temperature. The gray rectangles indicate the location of the three larger residence time channels. Cooling channel: water at 39 °C and flow rate > 80 ml/min. Reaction channel: ethanol at 10.6 ml/min (0.63 m/s). Modeling: see descriptions in the text.

When looking at the heat balance, the experiment can be described using the following simplified equations:

$$\begin{aligned} u \cdot \rho \cdot c_p \cdot \frac{dT}{dz} &= Ua_{global} \cdot \left(T - T_c\right) \\ \Rightarrow \frac{dT}{dz} &= \frac{Ua_{global}}{\rho \cdot c_p} \cdot \frac{1}{u} \cdot \left(T - T_c\right) \end{aligned} \tag{3}$$

Hence, assuming that the volumetric heat transfer coefficient Ua_{global} is identical in the mixing channel ($H \times W$ = 560 μm × 500 μm) and in the residence time channel ($H \times W$ = 560 μm × 2000 μm), one would expect a steeper temperature gradient dT/dz in the residence time channel due to the 4-fold reduced flow velocity. However, the curve obtained in Fig. 10 shows no clear difference between the larger residence time channels and the narrow mixing channels. From this observation, it was concluded that the volumetric heat transfer coefficient in the wider channels is about 4 times smaller than in the structured mixing channels. This difference was ascribed to two phenomena:

1) The presence of structures leading to an improved convection in the radial direction.
2) In spite of the fact that the heat exchange occurs mostly through the bottom of the reaction channel, due to the short distances, the side walls are not adiabatic. Hence, the specific heat exchange area is about 1.6-fold smaller for the wider channels.

For the modeling, a lumped volumetric heat transfer coefficient was calculated, assuming a uniform flow velocity in empty channels with a cross section of $H \times W$ = 560 mm × 500 mm all over the reactor. The value obtained for the mixing channels is $Ua_{global} = 1 \times 10^7$ W/(m^3 K) corresponding to a characteristic cooling time of $tc = \rho \cdot c_p / Uaglobal = 0.2$ s.

Furthermore, it has to be pointed out that the initial temperature in Fig. 10 differs from room temperature, as heat exchange occurs within a length of 6 mm prior to the area monitored by the infrared camera.

The volumetric heat exchange coefficients obtained under different conditions are summarized in Fig. 11. Thereby, one has to point out that this kind of estimation leads to a limited precision of up to ±25% due to the low temperature gradients (<8 °C) as compared to the accuracy of the method of ± 1 °C.

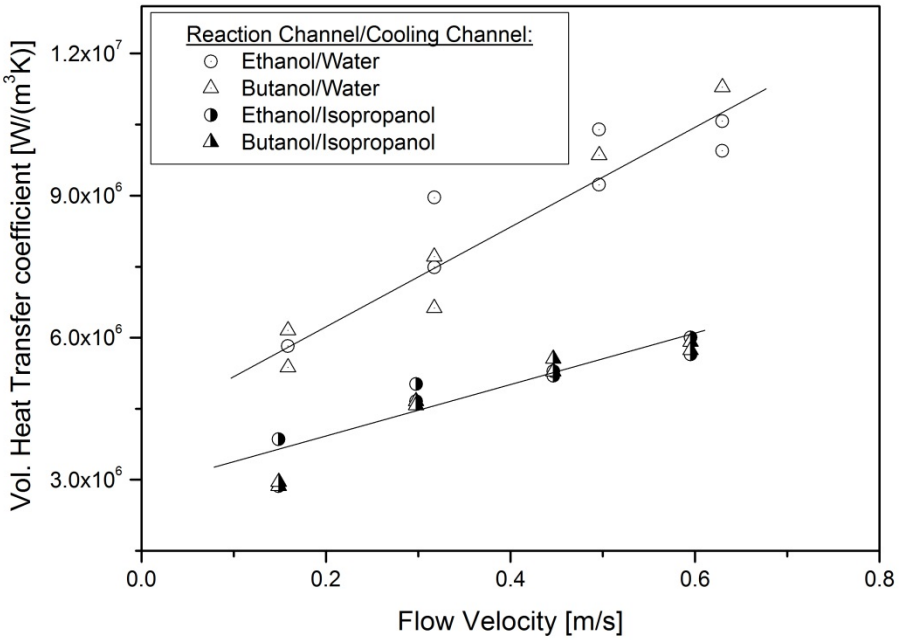

Figure 11: Comparison of the heat transfer coefficient estimated by heat exchange experiments with two different heat exchange media, i.e. water (λ_{H2O} = 0.638 W/(m·K)) and isopropanol (λ_{OH} = 0.138 W/(m·K)). The flow velocities are defined as the velocity after the third injection point.

Generally, the volumetric heat transfer coefficient is increasing with the flow rate which was varied up to 10.6 ml/min (0.63 m/s). The increased heat transfer was ascribed to the improved radial mixing with flow rate due to the herringbone structure, as demonstrated in the previous section. While changing the cold flow from ethanol to slightly more viscous butanol had no noticeable impact, the volumetric heat transfer coefficient in the working range (about 0.18 m/s corresponding to 3 ml/min) was improved almost 1.8-fold by changing from isopropanol to more heat conductive water as heat exchange medium.

By comparing the results obtained with isopropanol and with water, one can approximate the relative impact of the heat transfer resistance on the reaction layer and on the cooling layer side, respectively. The overall heat transfer resistance between reaction and cooling layer is described as follows:

$$1/Ua_{global} = R_{global} = R_{reaction} + R_{wall} + R_{cool} = \frac{1}{C'} + \frac{\delta}{\lambda_{wall}} \cdot a + \frac{1}{B \cdot \lambda_{fluid}} \quad (4)$$

Thereby, *C*' and *B* are two parameters describing the thermal resistance located on the reactor and on the cooling side, respectively. As with the available experiments the wall resistance cannot be distinguished from the reaction layer side resistance, both resistances are lumped into one constant *C*:

$$1/Ua_{global} \approx \frac{1}{C} + \frac{1}{B \cdot \lambda_{fluid}} \tag{5}$$

Thus, the ratio between the resistance obtained with isopropanol R_{OH} and with water R_{H2O} is:

$$\frac{R_{global,OH}}{R_{global,H2O}} = \frac{\frac{1}{C} + \frac{1}{B \cdot \lambda_{OH}}}{\frac{1}{C} + \frac{1}{B \cdot \lambda_{H2O}}} = \frac{1 + M/\lambda_{OH}}{1 + M/\lambda_{H2O}} \qquad \text{with} \qquad M = \frac{C}{B} \tag{6}$$

The ratio of both resistances obtained at a flow velocity of 0.18 m/s is 1.8 (see Fig. 11) giving a value of M = 0.18. Hence, the impact of the resistances can be determined as follows:

$$\frac{R_{reaction} + R_{wall}}{R_{cool,OH}} = \frac{\lambda_{OH}}{M} = 0.76 \tag{7}$$

$$\frac{R_{reaction} + R_{wall}}{R_{cool,H2O}} = \frac{\lambda_{H2O}}{M} = 3.54 \tag{8}$$

In the case of cooling with isopropanol more than 50 % of the resistance is located on the cooling layer side due to the larger channel and the absence of mixing structures. When changing the coolant to water, the resistance drops to about 20 % of the total resistance.

For the experiments described in the following sections, isopropanol was always used as a coolant allowing temperatures around 0 °C to be accessed. The coolant was fed with a minimum flow rate of 80 ml/min leading to a maximal temperature difference of 4 °C between inlet and outlet.

3.3 Temperature effects on the MI-MSR performance

In the following, the temperature profile of the multi-injection MSR under reactive conditions is presented. After demonstrating the good thermal control achieved in this type of equipment, the product distribution at different temperatures is discussed.

3.3.1 Enhanced temperature control in the MI-MSR

By taking the average temperature over the cross section, the 1-dimensional temperature profile was deduced (Fig. 12). As expected, temperature rises along the three herringbone mixers and decreases in the residence time channels. However, especially for the first mixing structure located in the bottom of the picture, a wavelike increase of temperature is observed: the three temperature minima are reached at the positions close to the cold reactor edge, whereas the maxima are reached when the flow passes through the regions located close to the center of the plate. In fact, the cooling is more effective on the reactor edge due to increased heat losses compared to the reactor center where slight thermal interactions between the channels cannot be neglected. Furthermore, after each injection point the hot spot is reached just in the beginning of the residence time channel, which is due to the about 4-fold reduced volumetric heat transfer coefficient in combination with ongoing mixing/reaction.

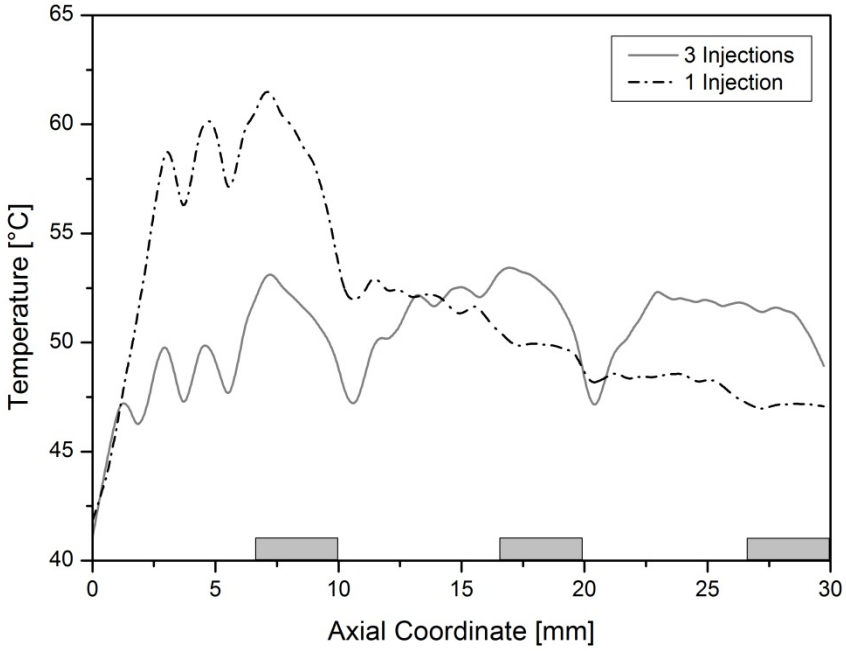

Figure 12: Axial temperature profile during the cyclization of pseudoionone in the MI-MSR with one injection point and with three injection points. Initial concentration of the two inlet solutions: c_{H2SO4} = 7.5 M and c_{PI} = 1.5 M; Total flow rate: 3 ml/min (0.18 m/s); ΔT_{ad} = 48 °C; T_{cool} = 48 °C. The gray rectangles indicate the location of the three larger residence time channels.

Using the MI-MSR, the temperature rise can be kept below 6 °C compared to the cooling temperature, which is the equivalent of an 8-fold reduced hot spot temperature compared to the adiabatic temperature rise ((54–48 °C)/48 °C = 1/8). The low hot spot is mainly attained due to three effects:

1) The high heat transfer coefficient attained in microchannels
2) The gradual mixing in the herringbone structure leads to a decelerated release of heat, thus, reducing the overall transformation rate.
3) The injection of pseudoionone at three distinct injection points.

3.3.2 Product distribution at different temperatures

The flow rate was kept constant at a total of 3 ml/min corresponding to a residence time of $\tau_1 \approx 4.1$ s for the molecules entering via the first injection point, of $\tau_2 \approx 2.5$ s for the molecules entering via the second injection point and $\tau_3 \approx 1.1$ s for the molecules entering via the third injection point. Simultaneously, the temperature in the cooling unit was varied between 0 °C and 80 °C with a maximum difference between inlet and outlet of 4 °C at 80 °C. The yields obtained are depicted in Fig. 13.

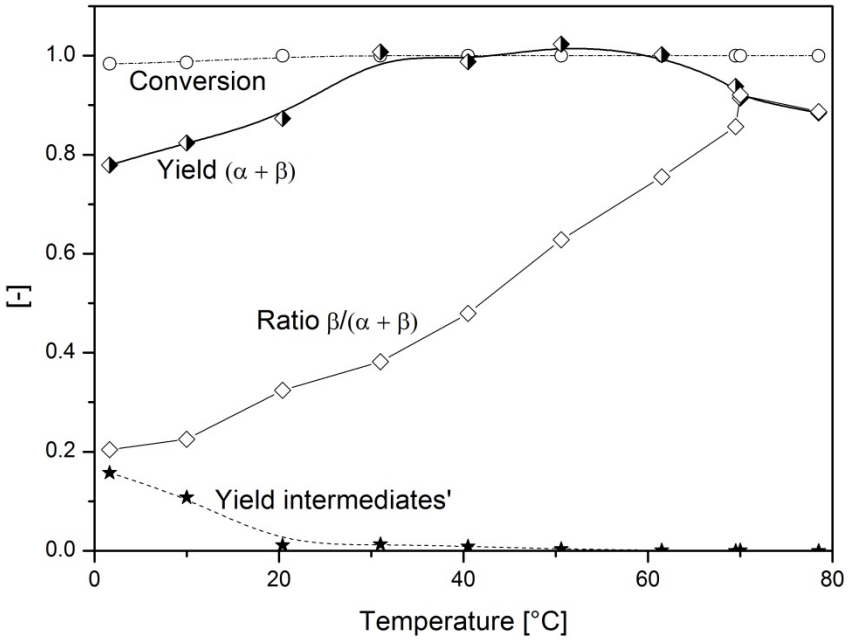

Figure 13: Yield and conversion at the outlet of the MI-MSR during cyclization of pseudoionone as function of coolant temperature. Thereby α and β denote α-ionone and β-ionone, and intermediates' are two isomers of 6,10-dimethylundeca-3,5-dione-10-hydroxy-2-one. Total flow rate: 3 ml/min (0.18 m/s), initial concentrations of the respective solutions: c_{PI} = 1.25 M; c_{H2SO4} = 7.5 M.

The conversion of the reactants is close to 1 all over the temperature range, indicating almost complete mixing of the reactants. The yield of the sum of α-ionone and β-ionone is 80% at temperatures around 0 °C and increases until a plateau of $Y_{\alpha+\beta} > 98\%$ reached at 30 °C. This yield is constant in the range of 30 °C to 60 °C, which constitutes an optimal operation window. From the large operation window of 30 °C, one can conclude that this particular model reaction does not necessarily need the high degree of temperature control as offered by this particular MI-MSR. The channel size could be further scaled up until a tolerance of almost 30 °C is attained, thereby benefiting from the higher throughput compared to a single injection reactor.

At low temperature, the deficit of $Y_{\alpha+\beta}$ accompanied by the appearance of intermediates can be attributed to a reduced transformation rate. For the deficit at temperatures above 60 °C, no intermediates are found in the outlet stream. Hence, one can conclude that the unwanted consecutive polymerization reaction takes place. The short residence time of this microstructured reactor allows working at much higher temperatures compared to a classical batch system, where the residence time in the order of 1 h causes a loss of $Y_{\alpha+\beta}$ already at temperatures above 10 °C [14]. When looking at the product distribution between α-ionone and β-ionone, as expected, the ratio of β/(α + β) increases with temperature as the kinetics of the isomerization reaction are accelerated. Thereby, 80% α-ionone is obtained at temperatures around 0 °C and about 80% of β-ionone at 65 °C.

Compared to the semi-batch process with a residence time in the order of hours, a space-time yield improvement of a factor $\tau_{batch}/\tau_{Multi\text{-}injection} \approx 500$ is achieved due to the improved temperature control [5].

3.4 Reduction of solvent mass

As final step, the inlet concentrations were raised with the aim of reducing the required amount of the solvent 1-nitropropane and of the excess of sulfuric acid. This was done in two consecutive steps: (1) The concentration of the inlet solution of pseudoionone was approximately doubled from 1.25 M to 2.75 M

while raising the concentration of sulfuric acid from 7.5 M to 12 M. Thereby, the ratio of acid to pseudoionone was diminished from 6 to 4.4; (2) in a next step, the acid concentration was further reduced to 7.5 M yielding a ratio of acid:pseudoionone of 2.7. While increasing the inlet concentrations, on the one hand, the adiabatic temperature rise increases, rendering temperature control a key issue. This was easily overcome by the good thermal control in the MI-MSR which allowed the hot spot temperature rise to be kept below 10 °C with an adiabatic temperature rise above 80 °C. On the other hand, the elevated viscosity of the solution limits the throughput with the setup used, as pressure drops above 1 bar could not be realized with syringe pumps. The working conditions and the product distribution achieved are summarized in Table 2 and in Fig. 14.

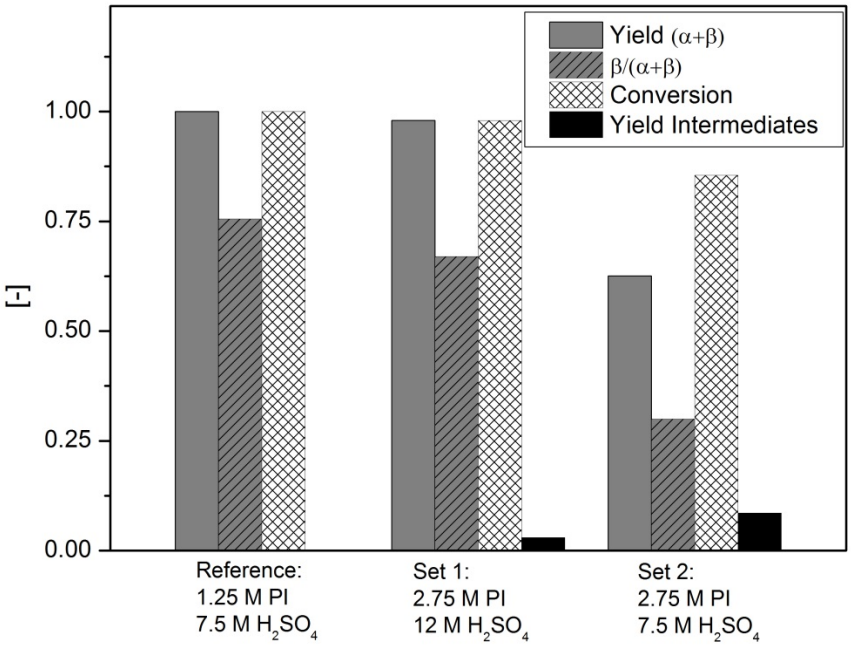

Figure 14: Yields and conversion obtained at the outlet of the MI-MSR during cyclization of pseudoionone. The respective experimental conditions are given in Table 2.

Table 2: Conditions used for comparison of the increased concentrations in Figure .

	Flow velocity [m/s]	**Coolant temperature [°C]**	**ΔT_{ad} [°C]**
Reference	0.18	60 °C	37 °C
Set 1	0.12	27 °C	81 °C
Set 2	0.18	27 °C	85 °C

When comparing the product quality of Set 1 to the Reference, an almost identical product distribution is observed with a slightly lower yield of β-ionone. The appearance of a non-negligible amount of intermediates can be linked to the reduced flow rate compared to the reference, and could be eliminated by increasing the flow rate with appropriate pumps. While changing from the reference to set 1, the required amount of solvent is reduced from 600 g/(l of solution) to 250 g/(l of solution).

A further reduction of the ratio sulfuric acid:pseudoionone as shown for Set 2 considerably reduces the yield of $Y_{\alpha+\beta}$ while an important amount of intermediates is found. This confirms the results published by

Kashid et al. [13] and [14], who showed that a ratio of acid:pseudoionone in the order of 5 is required for the reaction to complete.

4 Conclusion

The low temperature co-fired ceramics was shown to be a very suitable material for microstructured reactors due to high chemical resistance to harsh acidic and basic environments.

The temperature inside the MI-MSR was characterized via a quantitative IR thermography method. By measuring the temperature profiles under quasi-adiabatic conditions and deducing the mixing profile inside a tangential and a herringbone mixer, it was shown that the herringbone structure provides efficient mixing in a large range within the laminar flow regime (Re = 20‑130).

The incorporation of the herringbone structure within the MI-MSR enabled carrying out the highly exothermic and quasi-instantaneous model reaction of the cyclization of pseudoionone in the presence of concentrated sulfuric acid under continuous flow. The reduction of the hot spot temperature was 8-fold as compared to conventional batch reactors, where near adiabatic temperature rise is obtained. The improved temperature control was ascribed to three aspects of this new micro-reactor:

(1) The high volumetric heat transfer coefficient attained in the microchannels ($Ua \approx 4 \times 10^6$ W/(m^3 K))
(2) The gradual mixing in the herringbone structure leads to a decelerated release of heat and thus, reducing the overall transformation rate.
(3) The injection of pseudoionone into a flow of sulfuric acid at three distinct points provided a 2-fold reduced hot spot temperature compared to an operation mode with one single injection point.

Using the MI-MSR, yield of α- and β-ionones of $Y_{\alpha+\beta} > 98\%$ was attained with a residence time of 4.1 s. More than 500-fold improved space-time yield was achieved as compared to the conventional semi-batch reactor with typical processing times in the order of hours. Furthermore, by doubling the reactants' concentrations, the solvent quantity required during the reaction was reduced by a factor of 2.

5 Acknowledgement

The authors acknowledge the financial support from the 7th European Framework Program COPIRIDE Project (Grant agreement number: CP-IP 228853-2) and Swiss National Science Foundation.

References

[1] J. Haber, M.N. Kashid, A. Renken, L. Kiwi-Minsker, Heat management in single and multi-injection microstructured reactors: Scaling effects, stability analysis, and role of mixing, Ind. Eng. Chem. Res., 51 (2012) 1474-1489.

[2] V. Hessel, Novel Process Windows – Gate to Maximizing Process Intensification via Flow Chemistry, Chem. Eng. Technol., 32 (2009) 1655-1681.

[3] V. Hessel, B. Cortese, M.H.J.M. de Croon, Novel process windows – Concept, proposition and evaluation methodology, and intensified superheated processing, Chem Eng Sci, 66 (2011) 1426-1448.

[4] A.-L. Dessimoz, C. Berguerand, A. Renken, L. Kiwi-Minsker, Kinetic and thermodynamic study of the aqueous Kolbe–Schmitt synthesis of beta-resorcylic acid, Chem. Eng. J., 200–202 (2012) 738-747.

[5] J. Haber, B. Jiang, T. Maeder, A. Renken, L. Kiwi-Minsker, Multi-injection Microstructured Reactor for Intensification of Fast Exothermic Reactions: Proof of Concept, Green Processing & Synthesis, submitted (2013).

[6] M.N. Kashid, A. Gupta, A. Renken, L. Kiwi-Minsker, Numbering-up and mass transfer studies of liquid–liquid two-phase microstructured reactors, Chem. Eng. J., 158 (2010) 233-240.

[7] E.V. Rebrov, J.C. Schouten, M.H.J.M. de Croon, Single-phase fluid flow distribution and heat transfer in microstructured reactors, Chem. Eng. Sci., 66 (2011) 1374-1393.

[8] P. Barthe, C. Guermeur, O. Lobet, M. Moreno, P. Woehl, D.M. Roberge, N. Bieler, B. Zimmermann, Continuous Multi-Injection Reactor for Multipurpose Production – Part I, Chem. Eng. Technol., 31 (2008) 1146-1154.

[9] D.M. Roberge, N. Bieler, M. Mathier, M. Eyholzer, B. Zimmermann, P. Barthe, C. Guermeur, O. Lobet, M. Moreno, P. Woehl, Development of an industrial multi-injection microreactor for fast and exothermic reactions - Part II, Chem. Eng. Technol., 31 (2008) 1155-1161.

[10] P. Cougnon, D. Dochain, M. Guay, M. Perrier, Real-time optimization of a tubular reactor with distributed feed, AIChE Journal, 52 (2006) 2120-2128.

[11] Y. Lu, A.G. Dixon, W.R. Moser, Y.H. Ma, Analysis and optimization of cross-flow reactors with distributed reactant feed and product removal, Catalysis Today, 35 (1997) 443-450.

[12] L. Falk, J.M. Commenge, Performance comparison of micromixers, Chem Eng Sci, 65 (2010) 405-411.

[13] M. Kashid, O. Detraz, M.S. Moya, I. Yuranov, P. Prechtl, J. Membrez, A. Renken, L. Kiwi-Minsker, Micro-batch reactor for catching intermediates and monitoring kinetics of rapid and exothermic homogeneous reactions, Chem. Eng. J., 214 (2013) 149-156.

[14] M.N. Kashid, I. Yuranov, P. Raspail, P. Prechtl, J. Membrez, A. Renken, L. Kiwi-Minsker, Cyclization of Pseudoionone to β-Ionone: Reaction Mechanism and Kinetics, Ind. Eng. Chem. Res., 50 (2011) 7920-7926.

[15] Verein Deutscher Ingenieure, VDI-Wäarmeatlas, VDI-Verlag GmbH, Düsseldorf 2002.

[16] J. Haber, Heat Management for Process Intensification of Fast Exothermic Reactions in Microstructured Reactors, EPF Lausanne, Lausanne, 2013.

[17] H. Birol, Fabrication of low temperature co-fired ceramic (LTCC)-based sensor and micro-fluidic structures, EPFL, Lausanne, 2007.

[18] T. Thelemann, M. Fischer, A. Groß, J. Müller, LTCC-based fluidic components for chemical applications, Journal of Microelectronics and Electronic Packaging, 4 (2007) 167-172.

[19] G.A. Groß, T. Thelemann, S. Schneider, D. Boskovic, J.M. Köhler, Fabrication and fluidic characterization of static micromixers made of low temperature cofired ceramic (LTCC), Chem Eng Sci, 63 (2008) 2773-2784.
[20] T. Maeder, C. Slater, B. Jiang, F. Vecchio, C. Jacq, P. Ryser, "3D structuration of LTCC and related technologies for thermal management and microfluidic structures", Informacije MIDEM - Journal of Microelectronics, Electronic Components and Materials 42 (4), 234-244, 2012.
[21] W. Zhang, R.E. Eitel, Biostability of low-temperature co-fired ceramic materials for microfluidic and biomedical devices, Int. J. Appl. Ceram. Technol., 9 (2012) 60-66.
[22] R. German, P. Suri, S. Park, Review: liquid phase sintering, J Mater Sci, 44 (2009) 1-39.
[23] K. Makarovič, R. Bermejo, I. Kraleva, A. Benčan, M. Hrovat, J. Holc, B. Malič, M. Kosec, "The effect of phase composition on the mechanical properties of LTCC material", International Journal of Applied Ceramic Technology, 10 (2013), pp. 449–457
[24] C. Bienert, A. Roosen, "Characterization and improvement of LTCC composite materials for application at elevated temperatures", Journal of the European Ceramic Society, 30 (2010), pp. 369–374
[25] V. Hessel, H. Lowe, F. Schonfeld, Micromixers - a review on passive and active mixing principles, Chem Eng Sci, 60 (2005) 2479-2501.
[26] C.P. Holvey, D.M. Roberge, M. Gottsponer, N. Kockmann, A. Macchi, Pressure drop and mixing in single phase microreactors: Simplified designs of micromixers, Chemical Engineering and Processing: Process Intensification, 50 (2011) 1069-1075.
[27] J. Lee, S. Kwon, Mixing efficiency of a multilamination micromixer with consecutive recirculation zones, Chem Eng Sci, 64 (2009) 1223-1231.
[28] A. Cantu-Perez, S. Barrass, A. Gavriilidis, Residence time distributions in microchannels: Comparison between channels with herringbone structures and a rectangular channel, Chem. Eng. J., 160 (2010) 834-844.
[29] R. Choudhary, T. Bhakat, R.K. Singh, A. Ghubade, S. Mandal, A. Ghosh, A. Rammohan, A. Sharma, S. Bhattacharya, Bilayer staggered herringbone micro-mixers with symmetric and asymmetric geometries, Microfluidics and Nanofluidics, 10 (2011) 271-286.
[30] S. Hossain, A. Husain, K.Y. Kim, Shape optimization of a micromixer with staggered-herringbone grooves patterned on opposite walls, Chem. Eng. J., 162 (2010) 730-737.
[31] S.P. Kee, A. Gavriilidis, Design and characterisation of the staggered herringbone mixer, Chem. Eng. J., 142 (2008) 109-121.
[32] M.S. Williams, K.J. Longmuir, P. Yager, A practical guide to the staggered herringbone mixer, Lab Chip, 8 (2008) 1121-1129.
[33] A.D. Stroock, S.K.W. Dertinger, A. Ajdari, I. Mezić, H.A. Stone, G.M. Whitesides, Chaotic Mixer for Microchannels, Science, 295 (2002) 647-651.
[34] V. Mengeaud, Design and characterisation of basic units for an electrochemical processing plant at the microscale, PhD thesis: 2819; EPFL; 2003.
[35] J. Haber, M.N. Kashid, N. Borhani, J. Thome, U. Krtschil, A. Renken, L. Kiwi-Minsker, Infrared imaging of temperature profiles in microreactors for fast and exothermic reactions, Chem. Eng. J., 214 (2013) 97-105.